Copy No. _____

Defence Research and Development Canada
Recherche et développement pour la défense Canada

DEFENCE R&D DÉFENSE

Measured and modeled long-wave infrared signature of Quest in Q280

Zahir A. Daya
Daniel L. Hutt
Vincent Moura

Defence R&D Canada – Atlantic

Technical Memorandum
DRDC Atlantic TM 2007-309
March 2008

Canada

This page intentionally left blank.

Measured and modeled long-wave infrared signature of Quest in Q280

Zahir A. Daya
Daniel L. Hutt
Vincent Moura
Defence R&D Canada – Atlantic

Defence R&D Canada – Atlantic
Technical Memorandum
DRDC Atlantic TM 2007-309
March 2008

Principal Author

Original signed by Zahir A. Daya

Zahir A. Daya

Approved by

Original signed by Dave Hopkin

Dave Hopkin
Head/Signatures

Approved for release by

Original signed by James L. Kennedy

Head/Document Review Panel

Abstract

Canadian Forces Auxiliary Vessel (CFAV) Quest was imaged in the long-wave infrared (IR) band during DRDC Atlantic sea trial Q280 in February 2004. From images collected over several days, we have extracted the ship, sea and sky radiances. A contrast radiance between the ship and the background was calculated to determine the long-wave IR signature. Our analysis shows that the daytime signature of the vessel is larger than at night in the long-wave IR band. The contrast radiance of the stack exceeds that from the hull when contrasted against the winter sea. And finally, by comparing with prior studies, we note that the contrast ratio is larger in the mid-wave IR than in the long-wave IR when the contrast is constrained to the ship stack. We used ShipIR to model the Quest and its maritime environment. We found that the results were in general agreement with the measured data for both the sea and sky background and the ship surface. Overall, the typical difference between measured and modeled results was about $10-30\%$.

Résumé

Des images ont été prises du navire auxiliaire des Forces canadiennes (NAFC) QUEST dans l'infrarouge aux ondes longues durant l'essai en mer Q280 de RDDC Atlantique, en février 2004. Des images recueillies en plusieurs jours, nous avons extrait les intensités énergétiques du navire, de la mer et du ciel. Une intensité énergétique du contraste entre le navire et l'arrière-plan a été calculée pour déterminer la signature infrarouge aux ondes longues. Notre analyse montre que la signature de jour du navire est plus importante que la signature de nuit dans l'infrarouge aux ondes longues. L'intensité énergétique du contraste de la cheminée est supérieure à celle de la coque par rapport à la mer en hiver. Enfin, en faisant une comparaison avec les études antérieures, nous notons que le rapport de contraste est plus important à l'infrarouge aux ondes moyennes qu'à l'infrarouge aux ondes longues lorsque le contraste est limité à la cheminée du navire. Nous nous sommes servis du logiciel ShipIR pour modéliser le QUEST et son environnement maritime. Nous avons constaté que les résultats étaient généralement conformes aux données mesurées de la mer et du ciel à l'arrière-plan et de la surface du navire. Dans l'ensemble, l'écart-type entre les résultats mesurés et modélisés était normalement de 10 à 30%.

This page intentionally left blank.

Executive summary

Measured and modeled long-wave infrared signature of Quest in Q280

Zahir A. Daya, Daniel L. Hutt, Vincent Moura; DRDC Atlantic TM 2007-309;
Defence R&D Canada – Atlantic; March 2008.

Background: DRDC Atlantic trial Q280 was the first trial during which the CFAV Quest was imaged in the IR during the North Atlantic winter. Prior trials occurred during the early spring and mid-summer. The acutely different environment, with warm water relative to cold air, provided an alternative case to further understand IR signatures and develop modeling capabilities. As with other IR trials, the ship was imaged at 1 km range, cruising along a straight line at 10 knots, with mid- and long-wave cameras at small elevation angles.

The data analyzed here are limited to the long-wave but comparisons will be made to mid-wave data studied earlier. We report our analysis of measurements of the IR sea and sky backgrounds, and on the IR signature of the ship superstructure. We have used NTCS/ShipIR, a superior IR simulation code to model the IR signature of Quest during trial Q280. NTCS (Naval Threat Countermeasure Simulator) and its IR modeling module ShipIR are the NATO standard in IR modeling for ships.

Principal results: The background radiance characterized by the mean long-wave IR radiance as a function of the elevation angle has expected features from sea to sky. The data show that these vertical profiles vary significantly with the atmospheric temperature and with the extent of cloud cover. The measured profiles differ quantitatively from those modeled. In a qualitative sense the measured and modeled long-wave IR profiles are quite similar. The main quantitative differences are in the prominence of the IR radiance peak at the horizon and in the absolute value of the sea radiance: the model predicts too large of a peak and underpredicts the sea radiance.

The contrast between the radiances from the ship and from the sea increased from night to day. The stack invariably had a larger contrast than the hull. The contrast ratios suggest that the stack presents the greater vulnerability to the ship, especially during the day time. When compared with the mid-wave IR contrast ratios, we find that at ranges of about 1 km, the ship is in general more easily detected in the mid-wave than in the long-wave. This is particularly acute for the stack where the hot exhaust gases radiate in the mid-wave IR band. The greater risk posed by the stack in both IR bands strongly suggests that IR signature suppression should be a priority. Models were generally accurate with deviations of about $10-30\%$.

Future work: Presently, the political interest in the Arctic and possibly a future with active maritime trade at Arctic ports, heavily favors further research on IR signatures of ships in cold-water and wintry environments. Future DRDC Atlantic trials during the North Atlantic winter should be carried out to better gauge the range of the IR signature and to test the effectiveness of signature management equipment such as sea water injection to control stack signatures.

Sommaire

Measured and modeled long-wave infrared signature of Quest in Q280

Zahir A. Daya, Daniel L. Hutt, Vincent Moura ; DRDC Atlantic TM 2007-309 ; R & D pour la défense Canada – Atlantique ; mars 2008.

Introduction : L'essai Q280 de RDDC Atlantique était le premier durant lequel des images ont été prises du NAFC QUEST dans l'infrarouge dans l'Atlantique Nord en hiver. Les essais antérieurs avaient été menés au début du printemps et au milieu de l'été. Le milieu fort différent, avec de l'eau chaude par rapport à l'air froid, a constitué un autre cas permettant de mieux comprendre les signatures infrarouge et de mettre au point des capacités de modélisation. Comme à l'occasion d'autres essais relatifs aux signatures infrarouge, des images ont été prises du navire, qui se déplaçait en ligne droite à 10nœuds, à une distance de 1km, à l'aide de caméras à ondes moyennes et longues à de faibles angles de site. Les données analysées ici sont limitées aux ondes longues, mais des comparaisons seront faites avec des données sur les ondes moyennes étudiées plus tôt. Nous faisons état de notre analyse des mesures infrarouge de la mer et du ciel à l'arrière-plan et de la signature infrarouge de la superstructure du navire. Nous nous sommes servi du logiciel NTCS/ShipIR, code supérieur de simulation infrarouge, pour modéliser la signature infrarouge du QUEST durant l'essai Q280. Le NTCS (Naval Threat Countermeasure Simulator) et son module de modélisation infrarouge ShipIR constituent la norme de l'OTAN pour la modélisation des signatures infrarouge des navires.

Résultats : L'intensité énergétique de l'arrière-plan caractérisée par l'intensité énergétique infrarouge moyenne aux ondes longues en fonction de l'angle de site a des caractéristiques attendues à mesure qu'on passe de la mer au ciel. Les données montrent que ces profils verticaux varient de beaucoup en fonction de la température atmosphérique et de l'étendue de la couverture nuageuse. Les profils mesurés diffèrent quantitativement des profils modélisés. Sur le plan de la qualité, les profils infrarouge mesurés et modélisés aux ondes longues sont assez semblables. Les principales différences quantitatives se trouvent dans la prédominance des crêtes d'intensité énergétique infrarouge à l'horizon et dans la valeur absolue de l'intensité énergétique de la mer : le modèle laisse prévoir une crête trop grande et sous-estime l'intensité énergétique de la mer. Le contraste entre les intensités énergétiques du navire et de la mer a augmenté de la nuit au jour. La cheminée avait immanquablement un contraste plus marqué que la coque. Les rapports de contraste laissent entendre que la cheminée présente la plus grande vulnérabilité pour le navire, surtout le jour. Par rapport aux rapports de contraste infrarouge aux ondes moyennes, nous constatons qu'à des distances d'environ 1km, le navire est généralement plus facile à détecter aux ondes moyennes qu'aux ondes longues. C'est en particulier le cas de la cheminée, où les gaz d'échappement chauds

rayonnent dans l'infrarouge aux ondes moyennes. Le risque le plus élevé que pose la cheminée dans les deux bandes de l'infrarouge laisse fortement entendre qu'il faudrait accorder la priorité à la suppression de la signature infrarouge. Les modèles étaient généralement précis avec des écarts de 10 à 30%.

Recherches futures : À l'heure actuelle, l'intérêt politique manifesté envers l'Arctique et un avenir éventuel avec des échanges maritimes actifs dans des ports de l'Arctique favorise fortement d'autres recherches sur les signatures infrarouge des navires en eaux froides et dans des conditions hivernales. À l'avenir, les essais menés par RDDC Atlantique en hiver dans l'Atlantique Nord devraient être réalisés pour mieux établir la portée des signatures infrarouge et mettre à l'essai l'efficacité du matériel de gestion des signatures, comme l'injection d'eau de mer visant à limiter les signatures des cheminées.

Table of contents

List of figures

List of tables

This page intentionally left blank.

1 Introduction

The long-wave infrared (IR), that which is between about $8-12$ μm, has several military and civilian applications [1]. These include, for example, sensors for target detection and search and rescue cameras. In the naval sphere modern IR seeker missiles have become more sophisticated and earlier generations are more widely available. As a result they pose a threat to navy assets since ships can be detected in the IR against the sea or sky background. How readily the vessel is detected depends on the IR signature of the vessel and on the capability of the detector. From a ship defence perspective, it is important to quantify the IR signature for ships in the mid- and long-wave IR bands for different environments. For example, the winter North Atlantic climate differs from the summer North Atlantic in that the sea and air temperatures are often inverted, i.e., the air is colder than the sea.

In this report we study the IR signature of the Canadian Forces Auxiliary Vessel (CFAV) Quest during winter trial Q280. The IR signature is a contrast between the radiance of the ship and that from the background. During February 2004, CFAV Quest was imaged in the IR at a range of about 1 km off the Nova Scotia shore. Two IR cameras, one for the mid-wave and the other for the long-wave IR bands were used. The data analyzed here are limited to the long-wave but comparisons will be made to mid-wave data studied earlier [2].

We report our analysis of measurements of the IR sea and sky backgrounds, and on the IR signature of the ship superstructure. We have used NTCS/ShipIR, a superior IR simulation code to model the IR signature of the Quest during trial Q280. NTCS (Naval Threat Countermeasure Simulator) and its IR modeling module ShipIR are the NATO standard in IR modeling for ships. They have been developed in Canada by W. R. Davis Engineering Limited [3]. ShipIR accepts a set of input variables such as the air and sea temperatures, the relative humidity, the wind direction and speed, and the ship surface and exhaust plume properties to compute the IR radiance of the ship and its background. These input variables were measured during the trial.

Our analysis shows that the daytime signature of the vessel is larger than at night in the long-wave IR band. The contrast radiance of the stack exceeds that from the hull when contrasted against the winter sea. And finally, by comparing with prior studies, we note that the contrast ratio is larger in the mid-wave IR than in the long-wave IR when the contrast is constrained to the ship stack. For temporal variations in the radiance, our results show that the ship radiance differs statistically from the sea and sky radiances.

We used ShipIR to model the Quest and its maritime environment. We found that the results were in general agreement with the measured data for both the sea and sky background and the ship surface. Overall, the typical difference between measured and modeled results was about $10-30\%$.

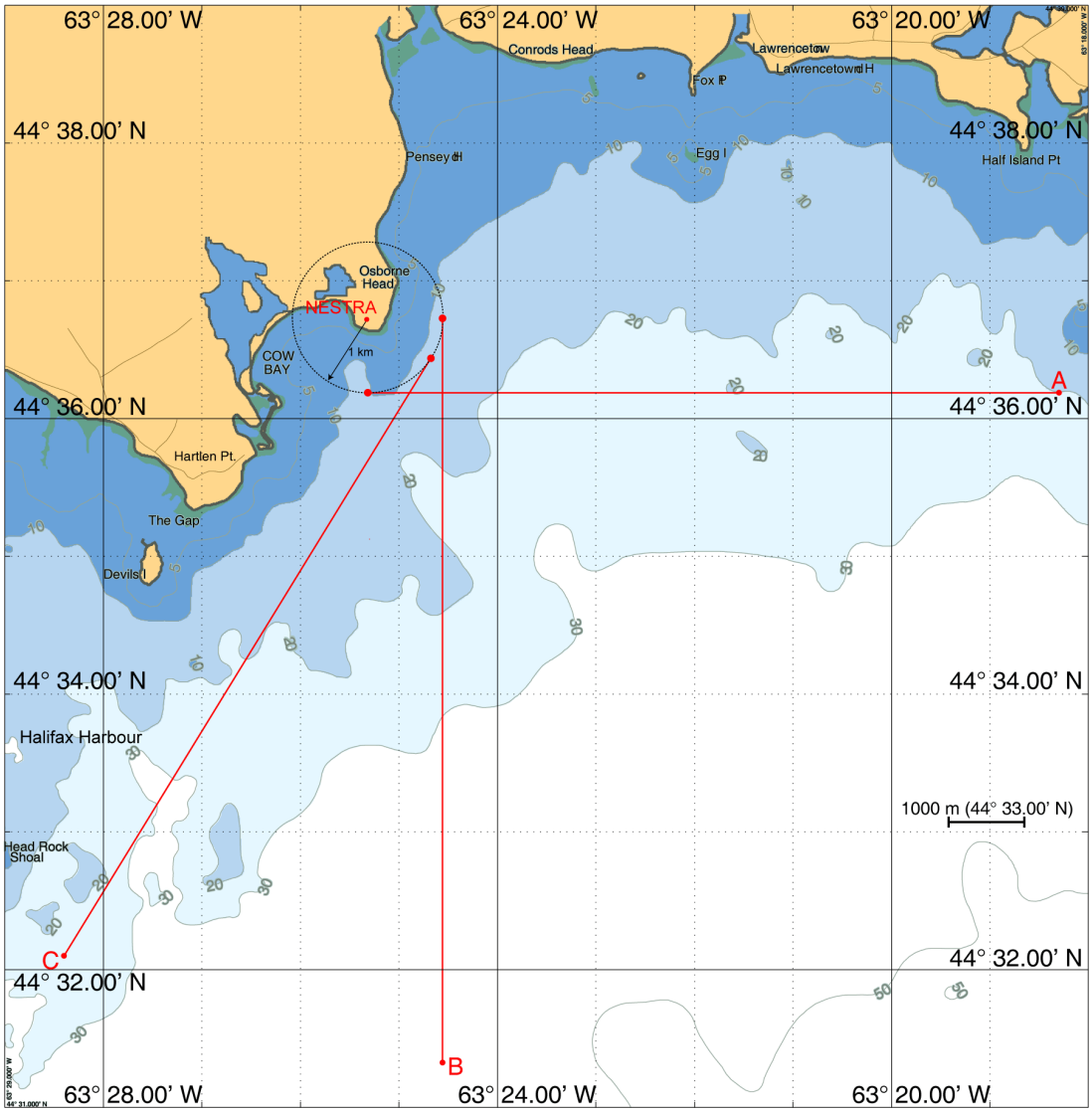

Figure 1: *A map of the trial area showing the Quest approaches for IR measurements during Q280.*

The remainder of this paper is organized as follows. The IR portion of trial Q280 is described in Section 2 and our analysis of the data are collected in Section 3. The ShipIR model is presented in Section 4, a comparison between long-wave and mid-wave IR signatures is given in Section 5, and a short conclusion follows in Section 6.

Figure 2: *A picture of the set-up of the IR cameras. Shown is Dr. David Vaitekunas of WR Davis Engineering who carried out the measurements*

2 Trial Q280 measurements

Measurements during the Quest trial Q280 were conducted off Osborne Head from the 16th to the 18th of February 2004. The objective was to study Quest's IR signature in a winter environment [4]. Mid- and long-wave IR cameras were located on shore at the NESTR-A (Naval Electronic Systems Test Range-Atlantic) facility at Osborne Head (44°36.8′N, 63°25.3′W). Each camera separately, filmed first the winter background without the ship and then the Quest at a range of about 1 km. These recordings consist of a collection of images.

Table 1: *Parameters of the mid- and long-wave IR cameras*

camera	FLIR S60/S65HS	FLIR SC1000
sensor type	bolometer	platinum-silicide
spectral range (μm)	$7.25-13.16$	$3.24-5.05$
size (W×H) in pixels	320×240	248×239
IFOV (*mrad*)	0.6677 ± 0.0020	0.7099 ± 0.0018
FOV (°)	$12.24^\circ\times9.18^\circ$	$10.09^\circ\times9.72^\circ$
calibration equation	$OS=a\cdot L+b$	$OS=a\cdot L^c+b$
calibration coefficients	$a=3.812624$ $b=11.00787$	$a=9030.049$ $b=654.3232$ $c=0.644677$

Table 2: *Configurations of selected IR runs from trial Q280.*

date	time (UTC)	run #	run type	solar azimuth	solar elevation	# of background images (time)	# of ship images (time)
Feb 16, 2004	23:09	8	C	179.8°	−18.2°	64 (10 sec)	182 (26 sec)
Feb 17, 2004	14:47	11	B	296.2°	29.4°	64 (10 sec)	175 (25 sec)
Feb 17, 2004	20:35	15	B	208.5°	10.1°	268 (57 sec)	186 (27 sec)
Feb 18, 2004	14:01	24	n/a	303.7°	27.4°	64 (10 sec)	n/a

In Fig. 1 we show a map of the trial area showing the location of NESTR-A and the several types of Quest runs for IR measurements. A picture of the camera set-up is shown in Fig. 2. The long-wave IR camera used during Q280 was the *S*65*HS* bolometer. It has a spatial field of 320×240 pixels and operates in the spectral range $7.25 - 13.16$ μm. With the lens, the long-wave camera had a field-of-view of $12.24^\circ \times 9.18^\circ$. The camera was calibrated on site against four black body panels spanning the temperature range of interest. The image data consists of the camera output signal (OS). The radiance L is obtained from the OS by a linear relation from a regression analysis of all the calibration data. The foregoing parameters and calibration relations for both the long- and mid-wave cameras are summarized in Table 1.

In a typical run, Quest would cruise at a constant speed of 10 knots, under diesel propulsion, for about a half-hour after which it would be imaged. The half-hour delay is to let the ship attain approximately steady thermal conditions. The cameras then acquired images at about $4 - 8$ Hz. For the current project, we have chosen to work on data from runs named Q280-run-8, -11, -15 and -24, since they coincide with mid-wave data analysis performed earlier [2] and so allow a direct comparison between the long-wave and mid-wave IR background radiances and ship signatures during the North Atlantic winter.

The four runs differ in run-type, in sky cover and in solar loading. Four IR run-types that are regularly executed in DRDC Atlantic trials [5] are shown in Fig. 1. Run Q280-run-8 was of type IR-C while Q280-run-11 and Q280-run-15 were of type IR-B. Q280-run-

Table 3: *Meteorological conditions during the runs.*

trial data set	air temperature	cloud cover	wind speed	wind direction	relative humidity
Q280-run-8	−10.3°C	clear	9.0 m/s	132°	48%
Q280-run-11	−9.5°C	clear	5.2 m/s	163°	50%
Q280-run-15	−2.5°C	clear	5.9 m/s	238°	48%
Q280-run-24	−5.7°C	cloudy	0.4 m/s	210°	75%

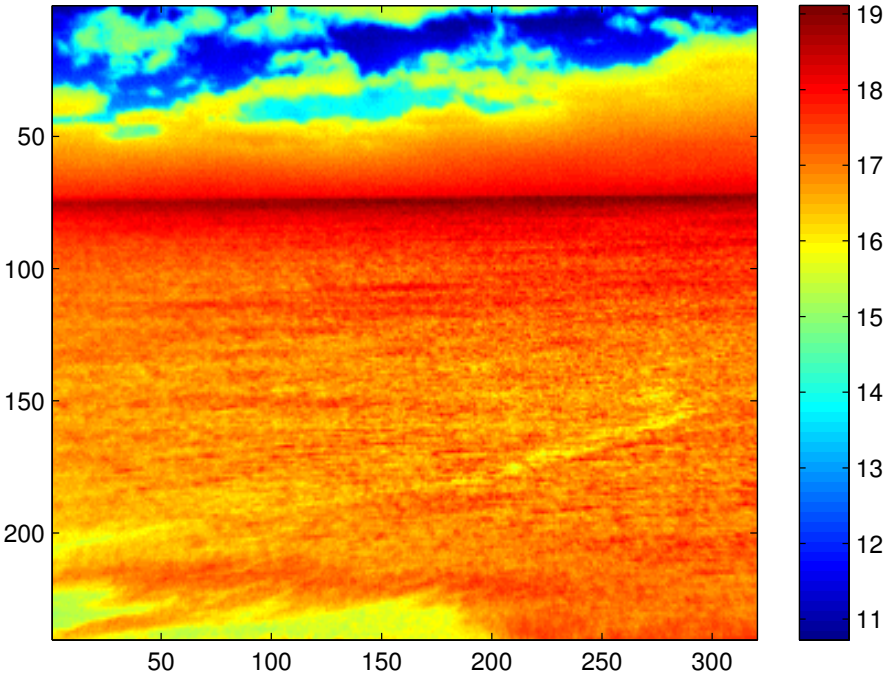

Figure 3: *Long-wave IR image of the background from Q280-run-8. The color bar shows the IR radiance in* $W/m^2/Sr$.

24 exclusively sampled the background. IR-B is a northbound run while IR-C is along heading 032°. Both types present the port side of the ship to the cameras. The date, time, run configuration and solar positions are summarized in Table 2.

The universal time tabulated indicates the beginning of the data acquisition for background images. The images for the ship follow those of the background. The background data were typically 10 seconds in duration acquiring about 60 images while the ship data spanned about 25 seconds and accumulated about 180 images. The solar positions (azimuth and elevation) were computed using NTCS/ShipIR for the mean time at which the ship was imaged during each run or for the mean time of the background images when the ship was not imaged.

Data for environmental variables such as temperature, wind speed and humidity amongst others were measured at the NESTR-A land station. These are summarized in Table 3. The temperatures and wind parameters were measured during the ship run. The air temperature, wind speed and direction were quite variable over time scales of a few minutes. The sea water temperature was approximately constant over several days during this trial averaging 0.05°C. Sea surface temperatures probably showed larger variation over the course of the trial but were not measured.

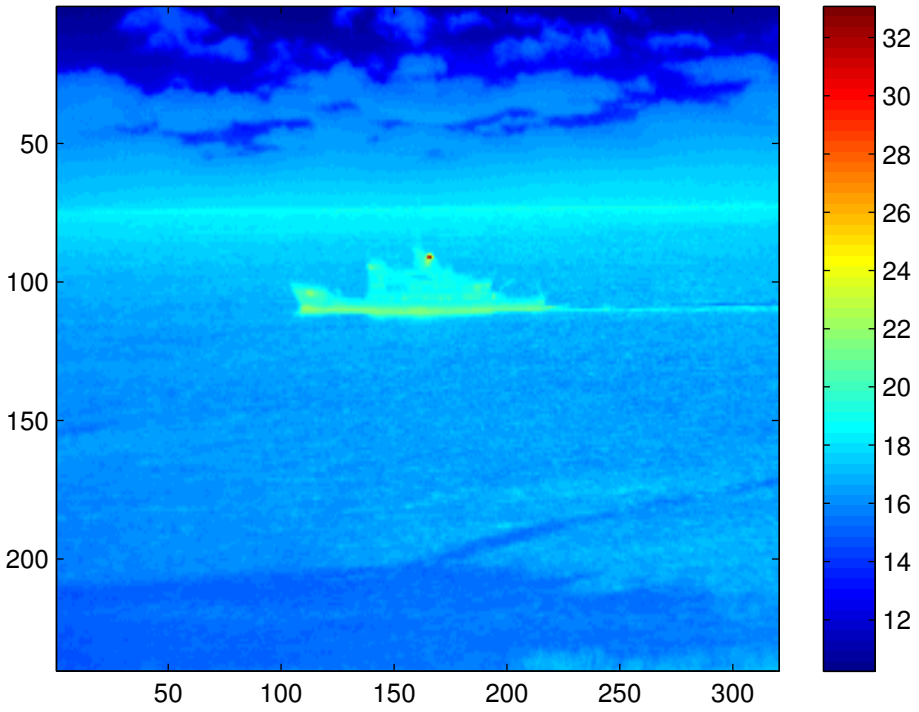

Figure 4: *Long-wave IR image of Quest from Q280-run-8. The color bar shows the IR radiance in* $W/m^2/Sr$.

The raw image data are converted from their native camera format into Matlab image matrices. The object signal data are then converted to IR radiances using the calibrations given in Table 1. The entire sequence of image data for each background or ship run is stored as a 3D array of 2D images. Typical images of the background and ship from the long-wave IR camera are shown in Figs. 3 and 4 respectively.

3 Data analysis and results

3.1 Long-wave IR radiance of the background

In this Section, we describe how the data are analyzed to extract background radiance and interpret the results. Systematic variation in the camera output was observed for the mid-wave camera in an earlier study [2]. Therefore, we were careful to study the long-wave data for systematic trends. As with the mid-wave camera, the long-wave data were also subjected to radial variation across the field-of-view. In Figs. 5 and 6 are shown two examples of the systematic radial variation in the camera radiance. In the former, we have

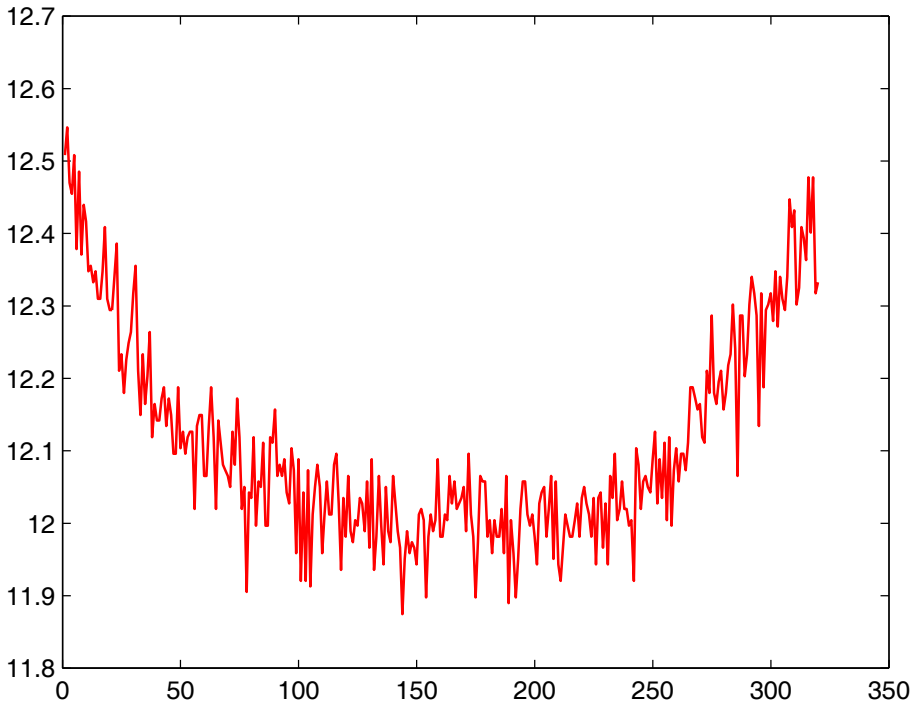

Figure 5: *Systematic variation of the radiance across the horizontal.*

extracted the radiance value across the horizontal from an image taken from Q280-run-11. Horizontal dependence is improbable across the limited field of view of the long-wave IR camera, hence, a flat response (up to noise) was expected. The data evidently shows that there is a systematic dependence in the radiance as one approaches the edges of the field of view. That this dependence is radial is seen by averaging several background images over a short duration (say 64 images over 10 seconds). In Fig. 6, we have plotted the average image of the background from Q280-run-24. Here, it is clear that the systematic variation in radiance is radially distributed.

The radial variation, as suggested earlier in Ref. [2], is probably due to thermal gradients on the camera lens and sensor assembly. Recall that the data were acquired in the winter when the cameras are likely to be exposed to thermal gradients. As shown in Fig. 6, cropping the central $6^\circ \times 6^\circ$ of the image results in a selection of data that is largely free of the radial variation. Additionally, other artifacts such as vegetation and a radar calibration pole that were sometimes in the field-of-view are avoided by the crop.

Of the original 320×240 pixels that span the entire image, the crop selects the central 156×156 pixels. These are divided between the sea and sky regions. The camera at NESTR-A is at an altitude of 26 m above sea level. Since the horizon is at the limit of

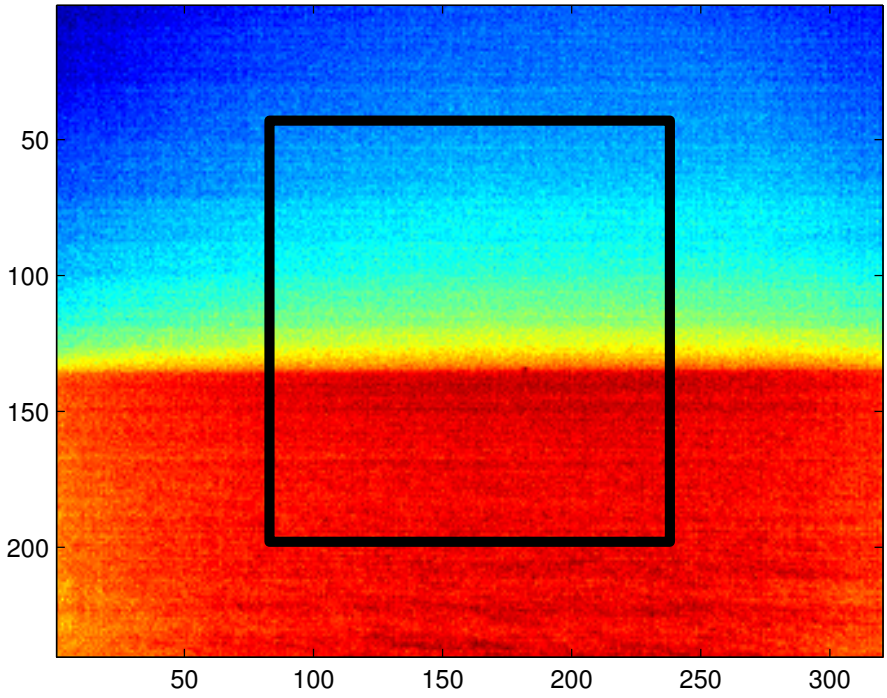

Figure 6: *A 10-second average image of the background (solid line:* $6^\circ \times 6^\circ$ *crop).*

visibility, typically about 20 km, we assume that it is located at an elevation angle of zero. For Q280-runs-8, -11, -15 and -24, the azimuth angle of the camera was constant. The elevation angle was changed during some of the runs so as to image upper reaches of the sky. The division into sea and sky regions resulted in the rectangular crops given in Table 4.

Mean long-wave IR radiance

In observing images of the background, we note that there is insignificant dependence of the background radiance on the azimuthal angle over the 6° field. Consequently, we average the radiance along each row for the columns of pixels within the crops. The resulting column, one from each background image, is a vertical profile of the average background radiance, i.e., the radiance as a function of the elevation angle. During each run, the background data were acquired as a sequence of images over a duration of about 10 seconds, which is sufficiently short so that it is statistically meaningful to average the background radiance from all the images in the sequence. The variation from image to image within this short duration are not due to diurnal effects but rather to fluctuations. Therefore averaging over the averaged background column from each image for all the images in each data set, we obtain the vertical profile.

Table 4: *Pixel dimensions of the sea and sky crops.*

trial data set	sky crop $W \times H$	sea crop $W \times H$
Q280-run-8	156×31	156×125
Q80-run-11	156×99	156×41
Q280-run-15	156×99	156×41
Q280-run-24	156×92	156×48

In Fig. 7, we have plotted the mean background radiance in the long-wave IR as a function of the elevation angle for each of the four data sets from trial Q280. The horizon is at an elevation angle of 0°, while the sky and sea span positive and negative angles respectively. The profile data show some common features: an almost constant sea radiance, a peak at the horizon and a decreasing radiance with increasing elevation angle in the sky. Furthermore, the data separate distinctly into clear and overcast cases. The clear sky cases Q280-run-8, -11 and -15, cluster together showing strong peaks at the horizon and rapidly decaying

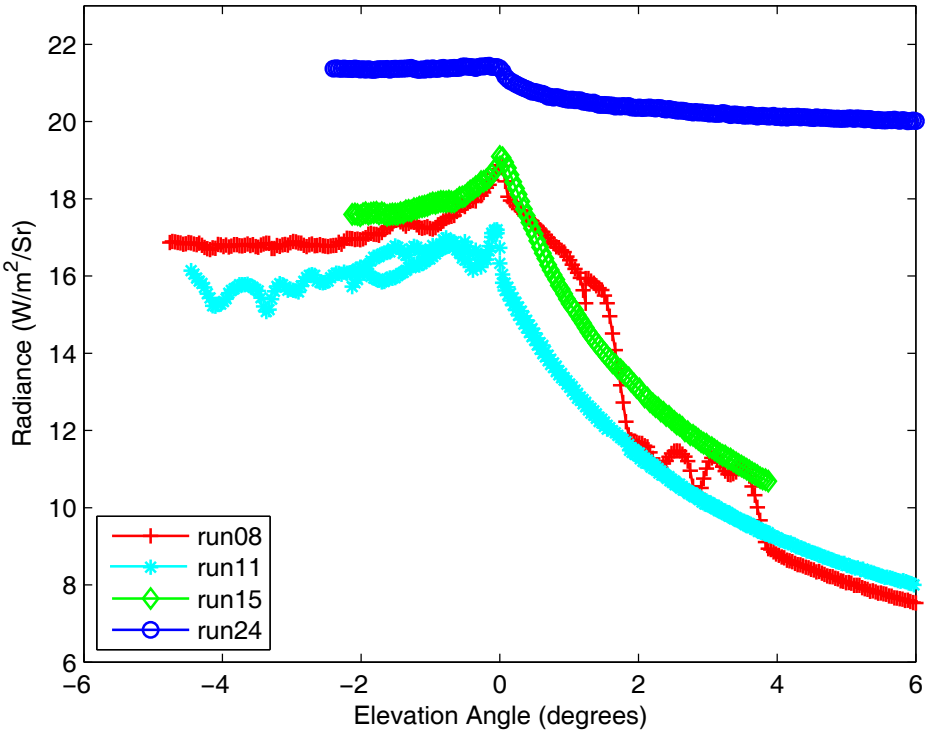

Figure 7: *Vertical profiles of the long-wave IR radiance for Q280-run-8, -11, -15 and -24. The horizon is at an elevation angle of* 0°*, sea at* $< 0^\circ$ *and sky at* $> 0^\circ$*.*

Table 5: *Mean and standard deviation of long-wave radiances of the sky and sea.*

trial data set	sky radiance		sea radiance	
	mean μ	rms σ	mean μ	rms σ
	$W/m^2/Sr$			
Q280-run-8	17.0	0.8	17.1	0.6
Q280-run-11	11.9	1.8	16.6	0.3
Q280-run-15	13.7	2.3	18.1	0.4
Q280-run-24	20.5	0.2	21.4	0.1

radiance in the sky. The out-of-trend variation in the sky radiance from the Q280-run-8 data is due to some broken clouds. The overcast data from Q280-run-24 shows a modest peak at the horizon and very slowly decaying radiance with increasing elevation angle in the sky. And, quite importantly, the radiance from the overcast case exceeds those from the clear sky data as is also the case in the mid-wave IR band [2].

The foregoing features in the background profile are largely expected. The local maximum in radiance from the horizon is due to the cumulative radiance from the line of sight to the horizon which has the thickest atmosphere. The decreasing radiance with increasing elevation angle results from the thinning of the atmosphere with altitude [6]. Cloudy or overcast skies have larger radiance due to the emission from the clouds and subsequent reflection off the sea surface [7]. The decrease in radiance with elevation angle on the cloudy day is very slight when compared to the clear sky runs since the blanket cloud cover replaces the otherwise thinning atmosphere in clear conditions.

Averaging over the radiances within the sky and sea regions for the background images for each of the runs, we extract the mean and standard deviations of the long-wave IR radiance. These are given in Table 5. In obtaining these results, the sky region was typically less than 3° in elevation angle above the horizon and the sea region extended to about -3° below the horizon. While the standard deviation measures the variation in the sea region, it averages over the systematic decrease of radiance with elevation angle for the sky. Note that the analysis of Q280-run-11 and -15 that had clear skies have comparable means and rms values. The data from the overcast day Q280-run-24 has the largest mean radiance and the smallest rms radiance. Completely overcast skies have very small variation in radiance. Q280-run-8 with some broken clouds shows a higher mean radiance than the clear day runs and intermediate rms values.

Temporal fluctuations in the long-wave IR radiance

The time-sequenced images of the background allow us to compute fluctuations in the long-wave IR radiance from the sea and sky regions. By subtracting the first image from the second image in each pair of consecutive images, we obtain a pixel-by-pixel image of the

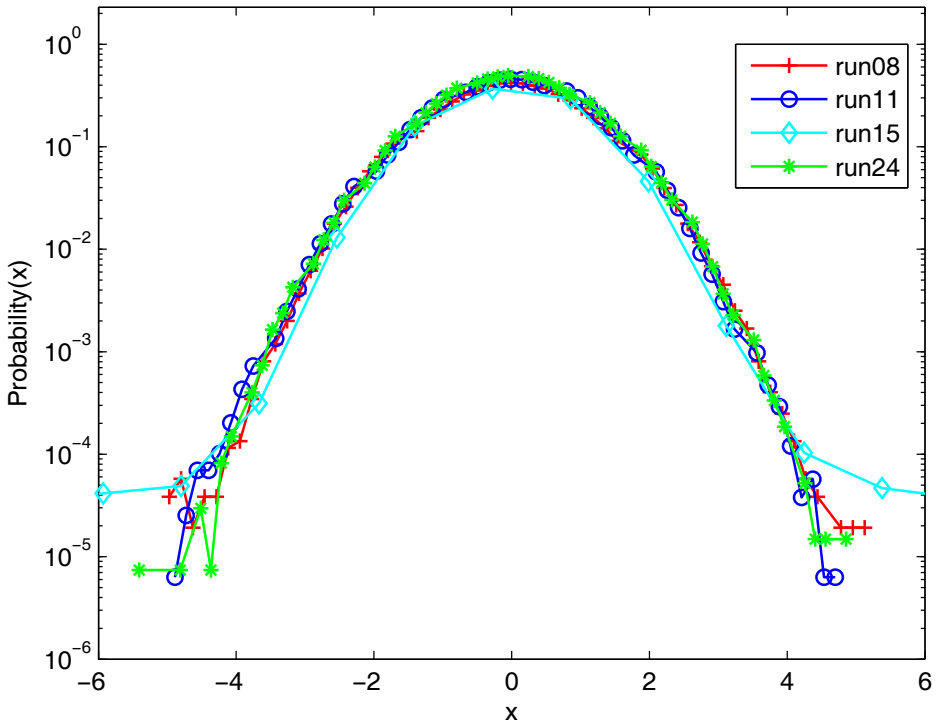

Figure 8: *The probability distribution of temporal fluctuations in the long-wave IR radiance of the sky. Here* $x = \frac{radiance-\mu}{\sigma}$*; each curve is deduced from the analysis of about* 10^6 *radiance data.*

fluctuations. Accumulating all the fluctuations from a data set in the sea and sky regions, we obtain a stochastic data set that characterize the variations of the long-wave IR radiance over frequencies of $4-8$ Hz. We cast the temporal fluctuations into a standard normal variable form by subtracting the mean and dividing by the rms. The means are approximately zero for both the sea and sky regions and for each of the data sets. The rms values averaged over the four data sets are $0.4\ W/m^2/Sr$ for the sky region and $0.06\ W/m^2/Sr$ for the sea region. The significantly larger rms for radiance fluctuations in the sky is due to air temperature variability arising from turbulent air movements. The relatively small rms for radiance fluctuations for the sea are due to a calm sea state, the relatively constant sea water temperature and the short line of sight between the sensor and the sea surface.

From the rescaled fluctuations, i.e., in standard normal variable form (zero mean and unit rms), we compute the probability distribution of the temporal fluctuations by common binning methods. In Figs. 8 and 9 we have plotted the probability distributions of the temporal fluctuations in the long-wave IR radiance for each of the four data sets for the sky and sea regions respectively. Our results show that the fluctuations in the sky and sea are largely Gaussian for fluctuations on time-scales of order 0.1 seconds. Departure

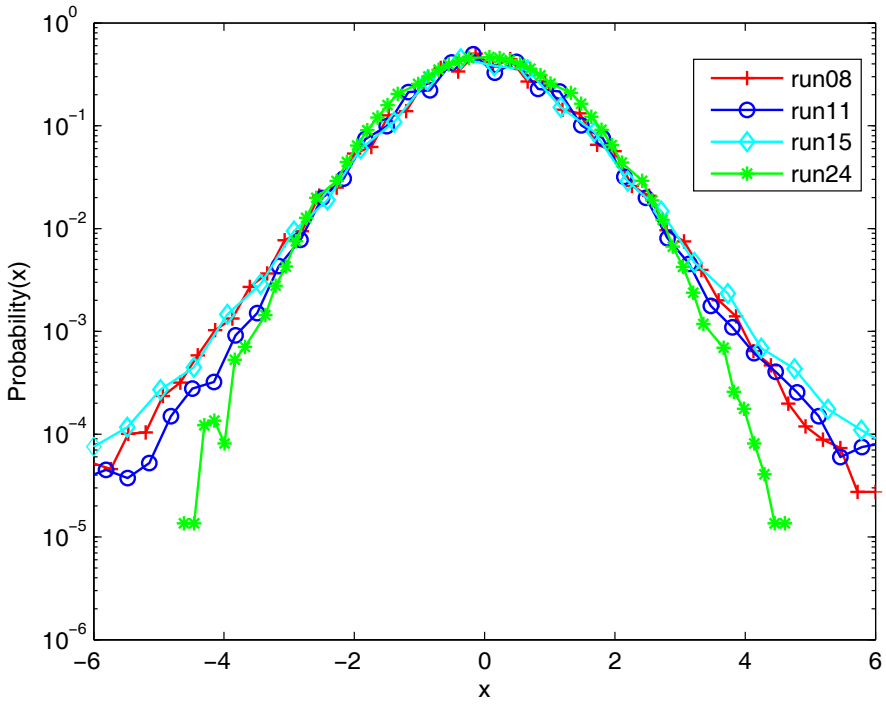

Figure 9: *The probability distribution of temporal fluctuations in the long-wave IR radiance of the sea. Here* $x = \frac{radiance-\mu}{\sigma}$*; each curve is deduced from the analysis of about* 10^6 *radiance data.*

from Gaussian behavior is noted in the tails of the probability distribution for the sea, more notably for clear sky data than for the overcast case. On repeating our analysis on fluctuations with larger temporal separations, say by subtracting the i^{th} image from the $i+2^{\text{th}}$ image or from the $i+4^{\text{th}}$ image, we find that the probability distributions are yet Gaussian suggesting that this behaviour extends to somewhat lower frequencies.

3.2 Long-wave IR radiance of the CFAV Quest in Q280

From simple observation of images of ships in the IR, it seems appropriate to describe the radiance from the ship by whether it originates from the the hot superstructure of the stack or the large flat plates that comprise the hull. The two regions appear to characterize the broadside exposure of the ship in the IR quite adequately. The stack is largely heated by engine exhaust and its temperature is moderated by the air flow around it. The hull though mainly in contact with air is also influenced by thermal contact with the sea water.

To proceed, we define two rectangular areas on the IR images of the CFAV Quest that demarcate the hull and stack regions. We will study the long-wave IR radiance that is observed to originate from these regions and how they contrast with the background radi-

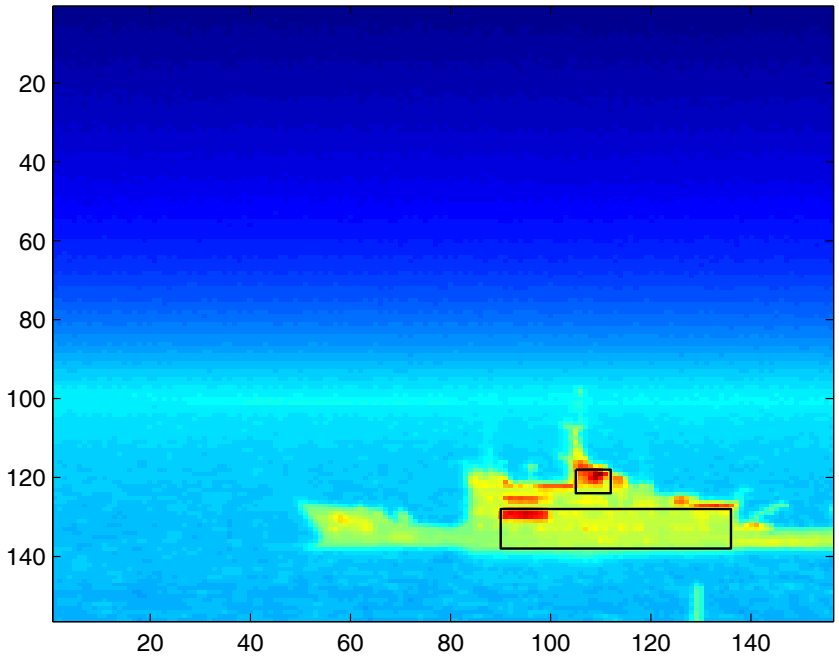

Figure 10: *Hull and stack regions on the ship are shown in black rectangles.*

ance. In Fig. 10 are shown the rectangles that define the hull and stack crops: these areas are fixed relative to the ship. The hull crop is 47×11 pixels spanning a physical area of about 200 m^2. The stack crop is 8×7 pixels and spans about 45 m^2.

Average long-wave IR radiances of the hull and stack regions

We have studied three data sets in which the CFAV Quest sails past the observation post at NESTR-A. Each of these data sets has about 180 images, all with clear sky conditions. From each image we have extracted the long-wave IR radiance values from the pixels within the stack and hull regions. The basic statistics, consisting of the mean and standard deviations in the long-wave IR radiance from the stack and hull are summarized in Table 6. Note that the mean radiance measured on the stack is about $5-10\%$ larger than on the hull for all the data sets. The rms deviations are $10-15\%$ of the mean on the stack but typically $5-10\%$ on the hull.

Table 6: *Mean and standard deviation of stack and hull radiances.*

trial data set	stack radiance		hull radiance	
	mean μ	rms σ	mean μ	rms σ
	$W/m^2/Sr$			
Q280-run-8	20.1	2.5	19.4	0.8
Q280-run-11	21.4	2.7	19.9	0.5
Q280-run-15	27.4	4.3	24.0	1.8

Temporal fluctuations in the long-wave IR radiance of the hull

Temporal fluctuations in the IR radiance from the hull region are calculated in the same manner as described earlier for the sea and sky backgrounds. From consecutive pairs of images, we subtract pixel by pixel, the radiance of the first image from the second to obtain the fluctuations on the hull region. As before, we cast the fluctuations into standard normal variable form and bin to obtain probability distributions. For the hull region and for each of the three data sets, we have plotted the probability distributions of the temporal fluctuations in Fig. 11. Unlike the sea and sky backgrounds, where the long-wave IR fluctuations are predominantly Gaussian, they significantly deviate from Gaussian form on the hull. The stack, consisting of only 7×8 pixels, and rather short sequence of images, does not accumulate enough fluctuation data to warrant generating probability distributions.

The long-wave IR contrast signature

The ability to visualize the ship is conferred by the different radiance levels between it and its background. Consequently, it has become common to refer to the difference or contrast as the IR signature of the ship. During trial Q280, the images of the Quest from Osborne Head contrast the hull and stack against the sea background. The altitude of the cameras at NESTR-A and the relatively short range to the ship do not offer contrasts against the sky. We define the long-wave IR contrast signatures for the hull and stack regions C_{hull} and C_{stack} as:

$$C_{\text{hull,stack}} = \mu_{\text{hull,stack}} - \mu_{\text{sea}}\,, \tag{1}$$

where the mean sea, hull and stack radiances are those summarized in Tables 5 and 6. The contrasts in Eq. 1 are often scaled by an intrinsic noise level, usually based on the sensor, known as the noise equivalent radiance. Here, we scale the contrasts by the mean background sea radiance and obtain simply a ratio of the contrast signatures to the background radiance:

$$R_{\text{hull,stack}} = \frac{C_{\text{hull,stack}}}{\mu_{\text{sea}}} = \frac{\mu_{\text{hull,stack}}}{\mu_{\text{sea}}} - 1\,. \tag{2}$$

The contrast radiances C_{hull}, C_{stack} and the contrast radiance ratios R_{hull}, R_{stack} for the CFAV Quest during trial Q280 are given in Table 7. Two observations that we make are

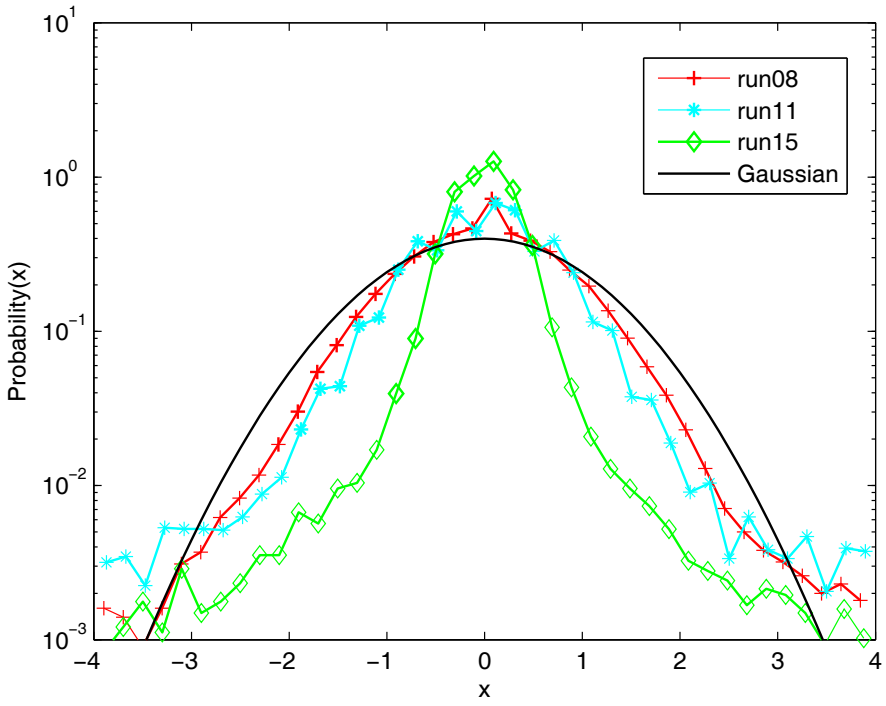

Figure 11: *Probability distribution of the temporal fluctuations in the long-wave IR radiance from the hull. Each curve is deduced from about* 10^5 *radiance data.*

the stack is more strongly contrasted than the hull and that the night-time data has a lower contrast than the day-time data. The rather striking difference amongst the two day-time data (Q280-run-11 and Q280-run-15) which were acquired on the same day but with solar elevations that saw a decline by about 20° and an air temperature that warmed by about 7°C. It is the reflection by the sea of the radiance emitted from the warmer air as to why the background sea radiance increases by about 8% from data set Q280-run-11 to Q280-run-15. It is this increase, which is not expected to be correlated with the changing solar elevation but rather due to the rapidly warming atmosphere, that results in the significantly different contrasts and contrast ratios.

Table 7: *Long-wave IR contrast radiances from the stack and hull regions.*

trial data set	C_{stack}	R_{stack}	C_{hull}	R_{hull}
	$W/m^2/Sr$		$W/m^2/Sr$	
Q280-run-8	2.98	0.17	2.22	0.13
Q280-run-11	4.77	0.29	3.26	0.20
Q280-run-15	9.35	0.52	5.95	0.33

4 IR modeling of the trial Q280 data

In this Section, we model the CFAV Quest and its background during trial Q280 with ShipIR and compare the results with our data analysis from Section 3. ShipIR is the IR modeling software module of NTCS, the Naval Threat and Countermeasure simulator developed by Davis Engineering Limited [3]. ShipIR/NTCS are the NATO standard in modeling ships in the infrared. ShipIR consists of several sub-models that model the sea, sky and ship with thermal and radiative balance equations. The sub-models are accessed by a graphical user interface that is also used to display the appearance of the ship and background in the IR.

4.1 Modeling the sea and sky background in the long-wave IR

The modeling process is quite involved. Here, we provide a brief description. The geographical location (latitude, longitude), calendar date and time of day are inputs that determine the sun's azimuth and elevation. An atmospheric model, in this case the standard North Atlantic Mid-Latitude Winter model, prescribes the shape of the temperature profile with altitude. The humidity, the sea and air temperatures are used to scale the profile of

Table 8: *Parameters for the ShipIR model of the background.*

trial data set	Q280-run-8 / Q280-run-11 / Q280-run-15
atmospheric model	mid-latitude winter
boundary layer	navy maritime
air mass parameter	2
cloud model	no clouds or rain
average wind speed	4.3 / 4.7 / 3.9 m/s
latitude	44.6°N
longitude	63.2°W
number of zenith points	18
number of azimuth points	36
sky type	lowmodtran
sea type	shaw
sea glint	normal
sun type	lowmodtran
scattering	multiple
observer altitude	26 m
observer IR band	6.993-13.986 μm
observer spectral response	FLIR S60/S65HS filter

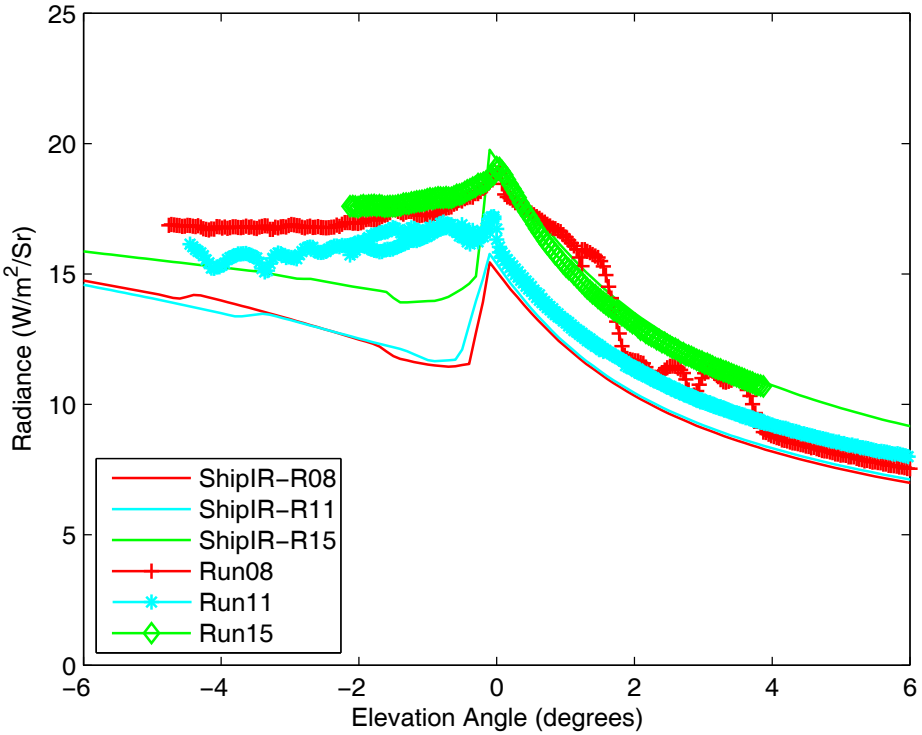

Figure 12: *Modeled and measured vertical profiles of the long-wave IR radiance.*

the atmospheric model. The sea surface is statistically modeled for a distribution of wave heights using the Shaw-Churnside distribution (ShipIR offers the user to select a model from several sea surface models). An average wind speed and air mass parameter are other inputs. The code is then used to calculate the background radiance for which the computational grid, the type of atmospheric scattering as well numerical convergence parameters can be chosen by the user. Atmospheric transmission of the IR radiation from the ship and background is handled by standard codes such as LOWTRAN [8] and MODTRAN [9] as selected by the user. The calculation has to take into account the location of the observer (the camera) and its spectral response. ShipIR can then be used to display the image that the observer would record. The parameters that were selected in modeling the data are summarized in Table 8. Other meteorological and chronological parameters were given earlier in Tables 2 and 3.

To compare the model to the data for the backgrounds, it is sufficient to study the vertical profiles, i.e., the average radiance as a function of elevation angle at a fixed azimuth. Using a built-in routine in ShipIR, we have extracted the long-wave IR radiance that would be observed by the camera as a function of elevation angle for the the three runs that have been modeled. Recall that the model takes into account the spectral response of the camera.

In Fig. 12, we have plotted the model predictions and the measurements. Overall, there is good agreement between the profiles from the data and model for the three runs. The model vertical dependence is systematically lower by about $5-15\%$ for elevation angles steeper than about $\pm 4^{\circ}$. Closer to the horizon and for shallow angle the difference between model and data can be as large as $20-40\%$. The rate at which the radiance decreases with increasing elevation angle matches very well between the model and the data. The qualitative agreement in the changes in the profiles from Q280-run-11 to Q280-run-15 driven by the warming air temperature are almost identical between the model and the data. However, the behaviour of the radiance from the horizon to the sea is rather different: the data show a small decrease from the horizon peak and approach to a constant value while the model predicts a sharper drop from the peak at the horizon followed by a steadily increasing sea radiance with more negative elevation angles.

4.2 Modeling the CFAV Quest in the long-wave IR

The target sub-model in ShipIR is used to configure the input parameters for the ship. A 3D CAD model of the ship has to be prepared for use with ShipIR. For the CFAV Quest, we have used a model "quest" created, under contract to DRDC Atlantic, by W. R. Davis Engineering Limited. Associated to the geometry are supplemental inputs that specify optical properties the outer surfaces of the ship and thermal parameters of the ship's plates and engine.

The optical surface properties (collected under the name "simvex" here) generally include a paint scheme for the ship with the spectral emissivities and directional reflectivities of the paints. The thermal parameters are the thermal conductivity, the heat capacities, the engine power, the exhaust flux temperature and constituent partial pressures (these are collectively known as "mp-runs"). Other parameters such as the wind speed and direction are used in

Table 9: *Parameters for the ShipIR model of the Quest.*

trial data set	Q280-run-8 / Q280-run-11 / Q280-run-15
geometry	quest
materials	simvex
spectral analysis	full spectral
plume	mp-runs
thermal boundary conditions	mp-runs
multi-bounce BRDF	on
bi-directional BRDF	on
speed	5.55 m/s
position (x,y,z)	(0,0,-5) m
yaw, pitch, roll	90(North), 0,0

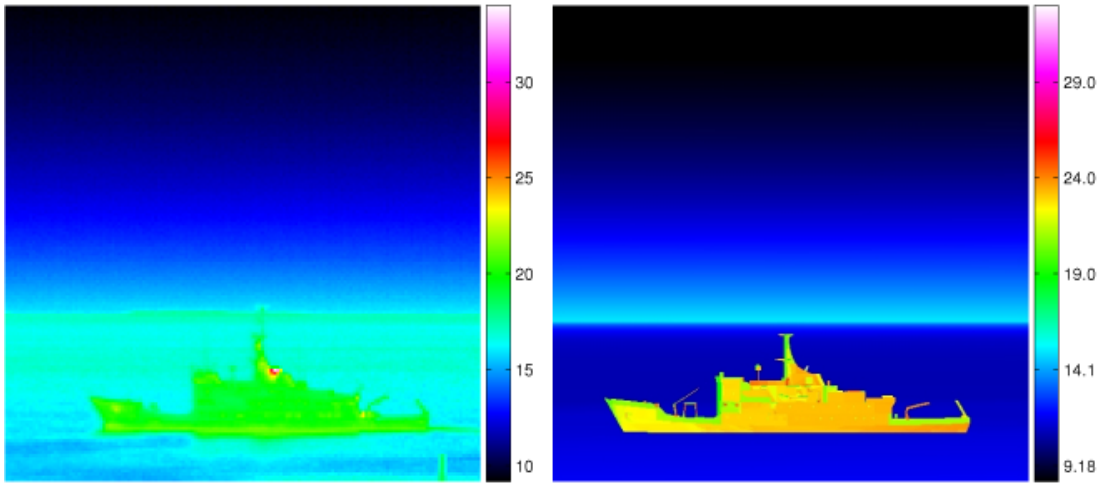

Figure 13: *IR radiance of the CFAV Quest: data versus model. The long-wave IR radiance measured in the data for Q280-run-11 (left) and predicted by its ShipIR model (right).*

modeling the convective cooling of the ship's surface. The target is then processed in the background to compute the observed radiance at the camera. A summary of some of the input parameters to ShipIR for the target model are given in Table 9.

A comparison between the measured long-wave IR radiance of the CFAV Quest and the prediction from the associated ShipIR model is shown in Fig. 13. There is generally good agreement qualitatively. Using image analysis tools in the ShipIR graphical user interface, we extract the mean radiances $\mu_{\text{hull,stack}}$ from the appropriate hull and stack regions defined in Fig. 10. We contrast the mean radiances against the average sea radiance to obtain the modeled IR contrast radiance and contrast radiance ratios, $C_{\text{hull,stack}}$ and $R_{\text{hull,stack}}$ defined in Eqs. 1 and 2. Our model results are summarized in Table 10. The modeled mean radiances from the stack and hull are systematically larger by about $10-20\%$ than those measured (see Table 6) for data sets Q280-run-8 and Q280-run-11. For Q280-run-15 for which the air temperature was increasing (note: this was the evening before snow storm "White Juan"), the data and model agree quite well for the hull but the model now underpredicts the stack radiance by about 10%. It appears to be generally true that the model and measurements are on average within $10-30\%$ for both the background and the ship.

Table 10: *Modeled long-wave IR contrast radiances from the stack and hull regions.*

model	μ_{stack}	C_{stack}	R_{stack}	μ_{hull}	C_{hull}	R_{hull}
	$W/m^2/Sr$	$W/m^2/Sr$		$W/m^2/Sr$	$W/m^2/Sr$	
Q280-run-8	23.6	12.0	1.03	24.2	12.6	1.09
Q280-run-11	24.3	12.0	0.98	24.1	12.3	1.04
Q280-run-15	24.2	9.7	0.67	24.4	9.9	0.68

It transpires, rather unfortunately, that the model's overprediction of the ship radiance and underprediction of the sea radiance result in contrast signatures that are $2-4$ times larger than those measured in the trial. Only for Q280-run-15, where the underprediction of the ship radiance, results in contrast radiances that are reasonably similar between the model and the measurements. The contrast ratios are comparable for Q280-run-15 but disparate for the other two runs. The model predictions suggest that the ship is equally vulnerable at night (Q280-run-8) as during day (Q280-run-11) with both stack and hull posing comparable risks. The measurements, as discussed earlier, suggest a higher risk from the stack and greater vulnerability during the day than at night.

5 Comparison between mid-wave and long-wave IR radiances

In this Section, we assess the similarities in the mid- and long-wave IR radiance of the background and the ship based on the measurements acquired during trial Q280. During the trial [4], the two IR cameras recorded the data almost simultaneously from approximately the same position at Osborne Head. As listed in Table 1, the field-of-views and pixel resolutions are quite similar.

In Figs. 14 and 15, we plot the vertical profiles of the background radiance in the long-wave and mid-wave IR bands respectively. The results for the mid-wave IR band are obtained from prior studies reported in Ref. [2]. Since there is more energy in the long-wave band of the electromagnetic spectrum than in the mid-wave band, we have roughly a factor of 10 between the absolute values of the radiance. The shapes of the vertical profiles and the trends in them are very similar between the two bands suggesting that the variations are due to physical phenomena that affect both bands similarly.

The background for data set Q280-run-24 had complete cloud cover: this results in the fairly constant sky radiance in both the mid-wave and long-wave data. Clear skies (or with some broken clouds) show a rapid decay of sky radiance with increasing elevation angle as noted in both bands for the other three data sets. In the mid-wave band the radiance of a clear sky decays by about 0.01 $W/m^2/Sr/deg$ while in the long-wave band the decay rate is about 3 $W/m^2/Sr/deg$ for small elevation angles near the horizon. These correspond to about $5\%/deg$ of the peak radiance in the mid-wave band and to approximately $15\%/deg$ of the peak radiance in the long-wave band.

The radiance from the sea and from the horizon show similar trends in both bands: the radiance is about constant from the sea and peaks at the horizon. The increase in sea radiance from clear to overcast conditions is about 30% in the long-wave band but only about 15% in the mid-wave band. Note that the cloud cover was accompanied with a 7°C warmer atmosphere. Temporal fluctuations in the sea and sky radiance are Gaussian distributed in

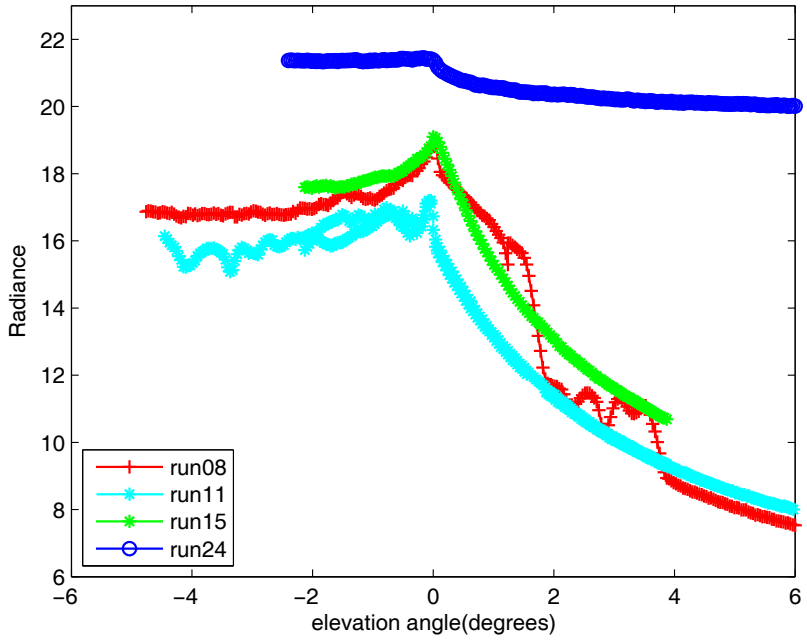

Figure 14: *Vertical profile of the background radiance in the long-wave IR band.*

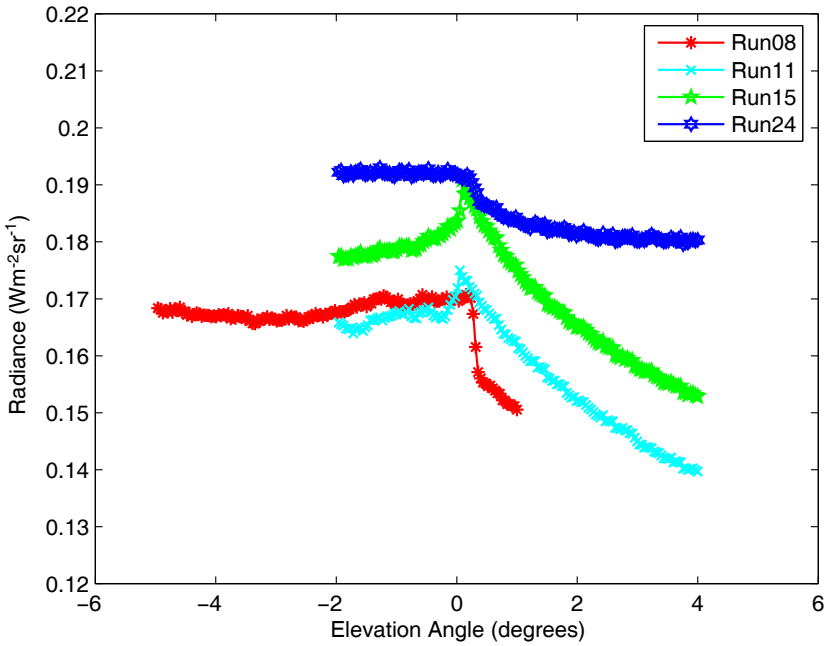

Figure 15: *Vertical profile of the background radiance in the mid-wave IR band.*

both the IR bands for time scales on the order of 0.1 seconds. The fluctuations had vanishing means and standard deviations that are about $1-2\%$ of the mean sky radiance. The fluctuations were smaller in the sea radiance.

The trends in the IR radiance from the ship and contrasts with the background are similar in the two IR bands. The mid-wave IR data studied previously overlapped the ship runs with data sets Q280-run-8 and Q280-run-15. It was found that the mid-wave IR radiance, the contrast against the sea, and the contrast ratios all increased from the night time (Q280-run-8) to the day time (Q280-run-15). In the long-wave IR band, this report shows the same trend with increasing ship radiances, contrasts and contrast ratios. The differences in the IR radiance from the stack and the hull are generally similar in both IR bands. Numerically, one cannot compare the radiance or contrast radiance between bands. However, we can compare the contrast radiance ratios which are non-dimensionalized against the radiance from the respective sea backgrounds.

The contrast ratios for the ship's stack (day and night time) and hull (day only) are larger in the mid-wave than in the long-wave IR band. The night-time hull contrast ratio is larger in the long-wave than in the mid-wave IR band based on a single measurement (Q280-run-8). The contrast ratios suggest that the CFAV Quest, in general, has larger peak signatures in the mid-wave IR than in the long-wave IR and thus a correspondingly larger vulnerability to detection by threats. The foregoing statements, needless to say, apply for the winter North Atlantic and under the specified environments.

6 Conclusion

DRDC Atlantic trial Q280 was the first trial for which the CFAV Quest was measured or imaged in the IR during the North Atlantic winter. The ship was imaged in the regular set of trial runs that had been developed for IR ranging: a 1 km range, cruising along a straight line at 10 knots, with mid- and long-wave cameras at small elevation angles. From the long-wave IR images, we have extracted the background radiance and contrasted the ship radiance against the sea.

The background radiance characterized by the mean long-wave IR radiance as a function of the elevation angle has expected features from sea to sky. The data show that the profiles vary significantly with the atmospheric temperature and with the extent of cloud cover. The measured profiles differ quantitatively from those modeled. In a qualitative sense the measured and modeled long-wave IR profiles are quite similar. The main quantitative differences are in the prominence of the IR radiance peak at the horizon and in the absolute value of the sea radiance: the model predicts too large of a peak at the horizon and underpredicts the radiance from the sea.

The contrast between the radiances from the ship and from the sea increased from night to day. The stack invariably had a larger contrast than the hull. The long-wave contrast ratios suggest that the stack presents the greater vulnerability to the ship, especially during the day time.

When compared with the mid-wave IR contrast ratios, we find that at ranges of about 1 km, the ship is in general more easily detected in the mid-wave than in the long-wave. This is particularly acute for the stack where the hot exhaust gases radiate in the mid-wave IR band. The greater risk posed by the stack in both the IR bands strongly suggests that IR signature suppression should be a priority if the CFAV Quest were a warship. Models for the radiance from the background and from the ship were generally accurate with deviations of about $10-30\%$.

Presently, the political interest in the Arctic and possibly a future with active maritime trade at Arctic ports, heavily favors further research on IR signatures of ships in cold-water and wintry environments. Future DRDC Atlantic trials during the North Atlantic winter should be carried out to better gauge the range of IR signature and to test the effectiveness of signature management equipment such as sea water injection to control stack signatures.

References

[1] Hackforth, H.L. (1960), Infrared Radiation, New York:McGraw-Hill Book Company, Inc.

[2] Z. A Daya, D. L. Hutt & J. R. Pelton (2007), Mid-wave IR signatures of the CFAV Quest in the North Atlantic Summer and Winter climates, (DRDC Atlantic TM 2007-312) Defence R&D Canada – Atlantic.

[3] D.A. Vaitekunas (2002), Technical Manual for ShipIR/NTCS (v2.9), Release Notes (v3.2).

[4] Hutt, D. L. (2005), Trials plan for CFAV Quest trial Q-280.

[5] Vaitekunas, D. A. (2005), Infrared signature instrumentation, measurement and modelling of CFAV Quest for Trial Q-280, *Document number A330-001, Rev 0*.

[6] Mermelstein, M. D. (1994), Midwave and long-wave infrared radiance and clutter at the ocean-sky horizon, *Optical Society of America, Vol. 19, No. 18*.

[7] M.A. Goforth, G. W. Gilchrist & J.D. Sirianni (2002), Cloud effects on thermal downwelling sky radiance, *SPIE Thermosense Conference Proceedings*.

[8] Air Force Research Laboratories, Space Vehicles Directorate (AFRL/VSBT)., LOWTRAN - Low spectral resolution atmospheric transmittance algorithm and computer model.

[9] Air Force Research Laboratories, Inc., Space Vehicles Directorate (AFRL/VSBT) in collaboration with Spectral Sciences, MODTRAN - Moderate spectral resolution atmospheric transmittance algorithm and computer model.

Distribution list

DRDC Atlantic TM 2007-309

Internal distribution

2 Authors
Attn: Zahir A. Daya, Daniel L. Hutt

5 Library

Total internal copies: 7

External distribution

Department of National Defence

1 DRDKIM
NDHQ/ADMS&T/DRDKIM

1 DSTM
NDHQ/CMS/DSTM

1 DSTM 3
NDHQ/CMS/DSTM 3
Attn: Greg Walker

2 DMSS 2
NDHQ/CMS/DMSS 2
Attn: Jan Czaban, Ping Kwok

2 DRDC Ottawa
3701 Carling Avenue, Ottawa, Ontario, K1A 0Z4
Attn: Satish Kayshap, Stephane Legault

3 DRDC Valcartier
2459 Pie-XI Blvd North, Qubec, Quebec G3J 1X5
Attn: Francoise Reid, Luc Forand, Denis Dion

Other Canadian recipients

1 David A. Vaitekunas
Senior Development Engineer
W.R. Davis Engineering Ltd

1260 Old Innes Road
Ottawa, Ontario
CANADA K1B 3V3

International recipients

1 Douglas Fraedrich
Naval Research Laboratory
Attn: Code 5757
4555 Overlook Ave., SW
Washington, DC 20375-5339 USA

1 Keith Youern
Defence Scientific and Technology Laboratory (Dstl)
Room C121 East Court, Portsdown West
Portsdown Hill Road
Fareham, Hants P017 6AD, England

Total external copies: 13

Total copies: 20

DOCUMENT CONTROL DATA

(Security classification of title, body of abstract and indexing annotation must be entered when document is classified)

1. ORIGINATOR (The name and address of the organization preparing the document. Organizations for whom the document was prepared, e.g. Centre sponsoring a contractor's report, or tasking agency, are entered in section 8.)

   Defence R&D Canada – Atlantic
   P.O. Box 1012, Dartmouth, Nova Scotia, Canada
   B2Y 3Z7

2. SECURITY CLASSIFICATION (Overall security classification of the document including special warning terms if applicable.)

   UNCLASSIFIED

3. TITLE (The complete document title as indicated on the title page. Its classification should be indicated by the appropriate abbreviation (S, C or U) in parentheses after the title.)

   Measured and modeled long-wave infrared signature of Quest in Q280

4. AUTHORS (Last name, followed by initials – ranks, titles, etc. not to be used.)

   Daya, Z.A.; Hutt, D.L.; Moura, V.

5. DATE OF PUBLICATION (Month and year of publication of document.)

   March 2008

6a. NO. OF PAGES (Total containing information. Include Annexes, Appendices, etc.)

   40

6b. NO. OF REFS (Total cited in document.)

   9

7. DESCRIPTIVE NOTES (The category of the document, e.g. technical report, technical note or memorandum. If appropriate, enter the type of report, e.g. interim, progress, summary, annual or final. Give the inclusive dates when a specific reporting period is covered.)

   Technical Memorandum

8. SPONSORING ACTIVITY (The name of the department project office or laboratory sponsoring the research and development – include address.)

   Defence R&D Canada – Atlantic
   P.O. Box 1012, Dartmouth, Nova Scotia, Canada B2Y 3Z7

9a. PROJECT NO. (The applicable research and development project number under which the document was written. Please specify whether project or grant.)

   11GS

9b. GRANT OR CONTRACT NO. (If appropriate, the applicable number under which the document was written.)

10a. ORIGINATOR'S DOCUMENT NUMBER (The official document number by which the document is identified by the originating activity. This number must be unique to this document.)

   DRDC Atlantic TM 2007-309

10b. OTHER DOCUMENT NO(s). (Any other numbers which may be assigned this document either by the originator or by the sponsor.)

11. DOCUMENT AVAILABILITY (Any limitations on further dissemination of the document, other than those imposed by security classification.)

   (X) Unlimited distribution
   ( ) Defence departments and defence contractors; further distribution only as approved
   ( ) Defence departments and Canadian defence contractors; further distribution only as approved
   ( ) Government departments and agencies; further distribution only as approved
   ( ) Defence departments; further distribution only as approved
   ( ) Other (please specify):

12. DOCUMENT ANNOUNCEMENT (Any limitation to the bibliographic announcement of this document. This will normally correspond to the Document Availability (11). However, where further distribution (beyond the audience specified in (11)) is possible, a wider announcement audience may be selected.)

13. ABSTRACT (A brief and factual summary of the document. It may also appear elsewhere in the body of the document itself. It is highly desirable that the abstract of classified documents be unclassified. Each paragraph of the abstract shall begin with an indication of the security classification of the information in the paragraph (unless the document itself is unclassified) represented as (S), (C), (R), or (U). It is not necessary to include here abstracts in both official languages unless the text is bilingual.)

Canadian Forces Auxiliary Vessel (CFAV) Quest was imaged in the long-wave infrared (IR) band during DRDC Atlantic sea trial Q280 in February 2004. From images collected over several days, we have extracted the ship, sea and sky radiances. A contrast radiance between the ship and the background was calculated to determine the long-wave IR signature. Our analysis shows that the daytime signature of the vessel is larger than at night in the long-wave IR band. The contrast radiance of the stack exceeds that from the hull when contrasted against the winter sea. And finally, by comparing with prior studies, we note that the contrast ratio is larger in the mid-wave IR than in the long-wave IR when the contrast is constrained to the ship stack. We used ShipIR to model the Quest and its maritime environment. We found that the results were in general agreement with the measured data for both the sea and sky background and the ship surface. Overall, the typical difference between measured and modeled results was about $10-30\%$.

14. KEYWORDS, DESCRIPTORS or IDENTIFIERS (Technically meaningful terms or short phrases that characterize a document and could be helpful in cataloguing the document. They should be selected so that no security classification is required. Identifiers, such as equipment model designation, trade name, military project code name, geographic location may also be included. If possible keywords should be selected from a published thesaurus. e.g. Thesaurus of Engineering and Scientific Terms (TEST) and that thesaurus identified. If it is not possible to select indexing terms which are Unclassified, the classification of each should be indicated as with the title.)

infrared signatures
long-wave IR
mid-wave IR
IR sensors
IR contrast

This page intentionally left blank.

Defence R&D Canada

Canada's leader in defence
and National Security
Science and Technology

R & D pour la défense Canada

Chef de file au Canada en matière
de science et de technologie pour
la défense et la sécurité nationale

www.drdc-rddc.gc.ca